Modeling frictional contact conditions with the penalty method in the extended finite element framework

Ewen Biotteau, Ponthot Jean-Philippe

▶ **To cite this version:**

Ewen Biotteau, Ponthot Jean-Philippe. Modeling frictional contact conditions with the penalty method in the extended finite element framework. ECCOMAS 2012, Sep 2012, Vienna, Austria. pp.MS119. hal-00731710

HAL Id: hal-00731710
https://hal.science/hal-00731710

Submitted on 13 Sep 2012

HAL is a multi-disciplinary open access archive for the deposit and dissemination of scientific research documents, whether they are published or not. The documents may come from teaching and research institutions in France or abroad, or from public or private research centers.

L'archive ouverte pluridisciplinaire **HAL**, est destinée au dépôt et à la diffusion de documents scientifiques de niveau recherche, publiés ou non, émanant des établissements d'enseignement et de recherche français ou étrangers, des laboratoires publics ou privés.

European Congress on Computational Methods
in Applied Sciences and Engineering (ECCOMAS 2012)
J. Eberhardsteiner et.al. (eds.)
Vienna, Austria, September 10-14, 2012

MODELING FRICTIONAL CONTACT CONDITIONS WITH THE PENALITY METHOD IN THE EXTENDED FINITE ELEMENT FRAMEWORK

E. Biotteau[1], **J.P. Ponthot**[1]

[1]University of Liège
LTAS Aerospace and Mechanics Department
Chemin des chevreuils, 1, building B52, 4000 Liège, Belgium
e-mail: ewen.biotteau,JP.Ponthot@ulg.ac.be

Keywords: extended finite element, frictional contact, penalty method, metal forming

Abstract. *This paper introduces an application of the eXtended Finite Element Method (X-FEM) to model metal forming processes. The X-FEM is used to account for material interfaces and reduce the meshing constraints due to the shape of the tools and the evolving configuration of the structures. Large deformations and non-linear behaviors are also accounted for, but this contribution focuses in the modeling of frictional conditions on the interface. In X-FEM simulations, the constraint of impenetrability is usually imposed using Lagrange multiplier methods. For such strategies, stabilisation algorithms are needed to prevent the apparition of instabilities due to the introduction of dual unknowns. The strategy presented here proposes to manage the contact using the penalty approach. As it requires no additional variables, it is not submitted to the same kind of instabilities. The contact problem is modeled using integration sub-elements, defined on the boundary of the structure, on which the contact constraints have to be enforced.*

1 INTRODUCTION

Despite the progresses in meshing and remeshing algorithms, metal forming problems are still very difficult to handle. In fact, realistic tool geometries lead to distorted elements which reduce the accuracy of the numerical model. To avoid the meshing constraints due to the deformation of the structure, meshless method can be usefull. The eXtended Finite Element Method [1] allows to build a numerical model without conforming the finite element edges with the structure boundary.

The X-FEM is used for a wide range of applications [2]. For material-void interfaces, the X-FEM enrichment only consists in multiplying the classical finite element shape functions with an Heavyside function which vanishes in the void [3]. However, as these enriched shape functions exhibit infinite gradients on the boundaries, specific integration strategies are needed (e.g. [4] and references therein).

In the context of contact problems, the relative displacements between the tool and the material play an important role on the metal flow and strongly influence the solution of the model, especially in case of frictional interfaces. In an X-FEM framework, the Lagrange multipliers method is widely used but requires stabilization strategies [5, 6]. In this contribution, the contact integration is performed using the penalty approach. To this end, an integration element which conforms to the boundary is created. On this integration element, the local penetration is computed at integration points and is turned into a contact pressure which will be integrated afterwards on the extended finite element. The main difficulty consists in finding the optimum penalty parameters.

The outline of this paper is as follows. In the next section, one reminds the contact formulation and the governing equations for large deformation analysis. Next, the discretization and the numerical integration within an X-FEM framework is presented. The last part of the paper presents some numerical two-dimensional simulations that validate the proposed strategy.

2 GOVERNING EQUATIONS IN NON LINEAR QUASI-STATIC ANALYSIS

One considers a body in its initial configuration Ω_0 with boundary Γ_0. In this reference configuration, the position of a material point is denoted by the vector $\underline{\mathbf{X}}$. On time t, the body occupies a domain Ω with boundary Γ. The position of the material point $\underline{\mathbf{X}}$ in the current configuration is denoted by $\underline{\mathbf{x}}$. The description of moving rigid tools is denoted by $\Upsilon(t)$.

One considers the problem of plane non-linear elastoplasticity under the quasi-static hypothesis. The unknowns are the displacement field $\underline{\mathbf{u}} = \underline{\mathbf{x}} - \underline{\mathbf{X}}$ and the Cauchy stress tensor $\underline{\underline{\boldsymbol{\sigma}}}$. One defines the deformation gradient $\mathbf{F}$ and the spatial gradient of velocity $\mathbf{L}$ as:

$$\mathbf{F} = \frac{\partial \underline{\mathbf{x}}}{\partial \underline{\mathbf{X}}} \quad \text{and:} \quad \mathbf{L} = \dot{\mathbf{F}}\mathbf{F}^{-1} \tag{1}$$

in the following, the symmetric part $\mathbf{D}$ (strain rate tensor) and the antisymmetric part $\mathbf{W}$ (spin tensor) of the spatial gradient of velocity $\mathbf{L}$ will be used to formulate the balance of the structure. Imposed displacement $\underline{\mathbf{u}}_{\mathrm{d}}$ and imposed surface tractions $\underline{\mathbf{t}}$ are respectively applied on the part Γ_{u} and Γ_{f} of the boundary. One denotes by Γ_{c} the complementary part of the boundary where contact conditions may be active. The governing equations in the current configuration are the following:

$$\begin{aligned} \mathrm{div}\left(\underline{\underline{\boldsymbol{\sigma}}}\right) + \underline{\mathbf{b}} &= \underline{\mathbf{0}} \quad \text{in } \Omega && (2)\\ \underline{\mathbf{u}} &= \underline{\mathbf{u}}_{\mathrm{d}} \quad \text{on } \Gamma_{\mathrm{u}} && (3)\\ \underline{\underline{\boldsymbol{\sigma}}}.\underline{\mathbf{n}} &= \underline{\mathbf{t}} \quad \text{on } \Gamma_{\mathrm{f}} && (4)\\ \underline{\underline{\boldsymbol{\sigma}}}.\underline{\mathbf{n}} &= \underline{\mathbf{f}} \quad \text{on } \Gamma_{\mathrm{c}} && (5)\\ \underline{\underline{\boldsymbol{\sigma}}}^{\nabla J} &= \mathbb{M} : \underline{\underline{\mathbf{D}}} \quad \text{in } \Omega && (6) \end{aligned}$$

where $\underline{\mathbf{b}}$, $\mathbb{M}$, $\underline{\underline{\mathbf{D}}}$ and $\underline{\mathbf{f}}$ represent respectively the body forces, the constitutive material tensor, the strain rate tensor and the contact forces. In large deformations, the time derivative of the Cauchy stress tensor in the constitutive law is replaced by the objective Jaumann rate $\underline{\underline{\boldsymbol{\sigma}}}^{\nabla J}$:

$$\underline{\underline{\boldsymbol{\sigma}}}^{\nabla J} = \underline{\underline{\dot{\boldsymbol{\sigma}}}} - \underline{\underline{\mathbf{W}}} : \underline{\underline{\boldsymbol{\sigma}}} + \underline{\underline{\boldsymbol{\sigma}}} : \underline{\underline{\mathbf{W}}} \tag{7}$$

Various approches are available in the literature to compute the contact load $\underline{\mathbf{f}}$. The treatment using the penalty approach will be detailed in the following sections and requires to compute the penetration between the tool and the deforming body.

For each point $\underline{\mathbf{x}}$ on the boundary, one defines as $\underline{\bar{\mathbf{x}}}$ the projection point on $\Upsilon(t)$. The normal gap g_n between the tool and the structure is defined as:

$$g_n = (\underline{\mathbf{x}} - \underline{\bar{\mathbf{x}}}).\underline{\mathbf{n}} \tag{8}$$

where $\underline{\mathbf{n}}$ represents the normal to the tool. The normal gap gives the contact status depending on its sign. If contact occurs ($g_n = 0$), a normal pressure $f_n < 0$ is induced. In the absence of contact ($g_n > 0$) the contact load is null. This leads to the so called Kuhn-Tucker conditions:

$$g_n \geq 0 \quad , \quad f_n \leq 0 \quad , \quad f_n g_n = 0 \tag{9}$$

If sticking or frictional contact is modeled, the tangential gap g_t must be accounted for. It is defined using the sliding path of the material particle on the tool:

$$g_t = \int_0^t \|\dot{g}_t\| \, dt \tag{10}$$

where $\dot{g}_t$ is the relative slip velocity.

3 THE DISCRETE PROBLEM

To formulate the discrete problem associated with the previous system of equations, let us denote as Θ the bounding box of the material domain Ω and Θ_e a discrete extended finite element (see figure 1).

Only two-dimensional problems are presently considered. The principles detailed below should be the same for three-dimensional examples and will be studied as perspectives of the current contribution.

3.1 Boundary description

The level set method [7] is used to implicitly represent the boundaries of the body and their evolution. The interface between void and material is described by the iso-zero of a function Ψ which represents the signed distance to the interface. The material part of Θ is such that $\Psi > 0$ while the void part is defined by $\Psi < 0$.

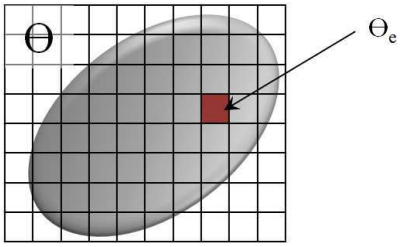

Figure 1: Subdivision of the bounding box Θ

In practice, the level set is evaluated at the nodes of Θ and is interpolated on the mesh using the finite element shape functions following:

$$\Psi(\mathbf{X},t)=\sum_{i=1}^{n}\Psi_I\left(t\right)\cdot\mathbf{N}_I\left(\underline{\mathbf{X}}\right)\quad\text{with: }\Psi_I=\pm\min\left\|\underline{\mathbf{x}}-\bar{\underline{\mathbf{x}}}\right\| \tag{11}$$

where Ψ_I represent the nodal value of the level set on node I and $\mathbf{N}_I$ the corresponding shape function. The nodal signed distance is computed using the projection $\bar{\underline{\mathbf{x}}}$ of $\underline{\mathbf{x}}$ on Υ. For complex structure geometry, one usually combines different level set corresponding to each merging interface. In this contribution, only one level set is used to find if a point lies inside or outside the material part. Later on, the interface position is computed accurately using the intersections between the curve describing the boundary of the structure and the elements edges.

3.2 X-FEM discretization

To manage the discontinuity inside the elements it is necessary to use special shape functions in the finite element approximation. In the case of discontinuities between void and material, the X-FEM consists in multiplying the classical finite element approximation with an Heavyside function $\mathbf{H}(\underline{\mathbf{x}})$ with value 1 if the point lies inside the material and 0 otherwise. The displacement field $\underline{\mathbf{U}}(\underline{\mathbf{X}},t)$ is interpolated as:

$$\underline{\mathbf{U}}(\underline{\mathbf{X}},t)=\sum_{I=1}^{n}\underline{\mathbf{U}}_I\left(t\right)\cdot\mathbf{N}_I\left(\underline{\mathbf{X}}\right)\mathbf{H}\left(\underline{\mathbf{X}}\right)=\sum_{I=1}^{n}\underline{\mathbf{U}}_I\left(t\right)\cdot\hat{\mathbf{N}}_I\left(\underline{\mathbf{X}}\right) \tag{12}$$

where $\underline{\mathbf{U}}_I\left(t\right)$ is the nodal value of the displacement. The discrete system of equations is obtained using the weak form of the equations to be solved:

$$\int_\Omega\frac{\partial(\delta\underline{\mathbf{u}})}{\delta\underline{\mathbf{x}}}\underline{\underline{\boldsymbol{\sigma}}}d\Omega=\int_\Omega\delta\underline{\mathbf{u}}\rho\underline{\mathbf{b}}d\Omega+\int_{\Gamma_\mathrm{f}}\delta\underline{\mathbf{u}}\,\underline{\mathbf{t}}dS+\int_{\Gamma_\mathrm{c}}\delta\underline{\mathbf{u}}\,\underline{\mathbf{f}}dS \tag{13}$$

Using the arbitrariness of the virtual test function $\delta\underline{\mathbf{u}}$ and the extended finite element discretisation (12) for both the displacement and the virtual test function, one gets:

$$\underline{\mathbf{F}}^i = \underline{\mathbf{F}}^e + \underline{\mathbf{F}}^c \tag{14}$$

$$\text{with:} \qquad \underline{\mathbf{F}}^i = \sum_{\Theta_e=1}^{n_e} \int_{\Theta_e} \frac{\partial \underline{\hat{\mathbf{N}}}}{\partial \underline{\mathbf{x}}} \underline{\underline{\boldsymbol{\sigma}}} d\Theta \tag{15}$$

$$\underline{\mathbf{F}}^e = \sum_{\Theta_e=1}^{n_f} \int_{\Gamma_{\mathrm{f}}^e} \underline{\hat{\mathbf{N}}}\, \underline{\mathbf{t}} dS \tag{16}$$

$$\underline{\mathbf{F}}^c = \sum_{\Theta_e=1}^{n_c} \int_{\Gamma_{\mathrm{c}}^e} \underline{\hat{\mathbf{N}}}\, \underline{\mathbf{f}} dS \tag{17}$$

where Γ_{f}^e and Γ_{c}^e denotes respectively the Neumann and contact parts of the boundary inside an element. This equation is iteratively solved using a Newton linearization procedure. It requires the computation of the tangent stiffness matrix associated with all the non-linearities. The contact problem formulation is detailed in the following subsection. The processing for other non-linearities will be detailed in a following contribution [8].

3.3 Contact Management

The contact conditions are accounted for using the penalty approach. As the contact is only weakly enforced, a negative gap (i.e. a penetration) is allowed between the tool and the structure. Using a contact material law, this gap is turned into a boundary stress which is integrated over the extended finite element.

The contact contribution is computed on a one-dimensional integration element which conforms to the boundary of the structure inside the extended finite element. In this one-dimensional element, one computes the gaps on each Gauss point using equations (8) and (10). These gaps are turned into a boundary stress using penalty parameters:

$$\underline{\mathbf{f}} = \mathrm{f_n}\underline{\mathbf{n}} + \mathrm{f_t}\underline{\mathbf{t}} \tag{18}$$

$$\text{with: } \mathrm{f_n} = \begin{cases} \epsilon_n g_n & \text{if: } g_n < 0 \\ 0 & \text{else} \end{cases} \qquad \text{and: } \mathrm{f_t} = \begin{cases} \epsilon_t g_t & \text{if: } g_n < 0 \\ 0 & \text{else} \end{cases} \tag{19}$$

In case of frictional contact, if the tangent stress overestimates the current sliding stress, depending on the contact material (for example a Coulomb law), one brings the tangential stress back to its maximum value:

$$\mathrm{f_t} = \begin{cases} \epsilon_t g_t & \text{if:} \quad |\epsilon_t g_t| < |\mu \epsilon_n g_n| \\ \pm \mu \epsilon_n g_n & \text{else} \end{cases} \tag{20}$$

where μ denotes the frictional coefficient. The sign of the corrected tangent stress is set to the sign of the overestimated tangent stress. It is important to notice that contrary to classical penalty methods generally used in a finite element context, penalty parameters do not turn the gap into a nodal force but into a boundary traction stress. Then, using equation (17) one integrates this load over the extended finite element discontinuity. To compute this integral, one uses a Gaussian quadrature rule on the one-dimensional integration element. The contact

contribution is given by:

$$\underline{\mathbf{F}}^c = \sum_{\Theta_e=1}^{n_c} \sum_{GP=0}^{n_{GP}} w_{GP} \hat{\mathbf{N}}\, \underline{\mathbf{f}}\, |J_{GP}| \tag{21}$$

In equation (21), the weight of the Gauss points and the Jacobian determinant are taken with respect to the one-dimensional element while the shape functions are computed using the reduced coordinate of the one-dimensional integration point in the two-dimensional extended finite element space. Using equation (21), even the nodes that lies outside the material (called phantom nodes) will get a contact load.

For solving the associated non-linear equilibrium, a linearization of the contact contribution is necessary and the tangent stiffness matrix associated with the contact must be computed. The material terms are given in the following. To simplify the explanation, the tangent stiffness matrix calculation is split between the normal and tangential parts. For the normal contribution, it is defined as:

$$K^n_{ikIJ} = \sum_{\Theta_e=1}^{n_c} \sum_{GP=0}^{n_{GP}} w_{PG} \psi^T_{iI} \psi_{jJ} \epsilon_n \, |J_{GP}| \tag{22}$$

where $\psi_{iI} = N_I n_i$. Function ψ is computed using the reduce coordinates of the Gauss points of the integration line in the quadrangular parent configuration. Once more, the jacobian determinant and the weight of the Gauss points are associated to the one-dimensional element. The tangent contribution to the stiffness matrix depends on the contact status and is defined as:

$$K^{con}_{ikIJ} = \begin{cases} \sum_{\Theta_e=1}^{n_c} \sum_{GP=0}^{n_{GP}} w_{PG} \hat{\psi}^T_{iI} \hat{\psi}_{jJ} \epsilon_t \, |J_{GP}| & \text{sticking contact} \\ \sum_{\Theta_e=1}^{n_c} \sum_{GP=0}^{n_{GP}} w_{PG} \hat{\psi}_{iI} \psi_{jJ} \mu \epsilon_n \, |J_{GP}| & \text{sliding contact} \end{cases} \tag{23}$$

with $\hat{\psi}_{iI} = N_I t_i$.

4 NUMERICAL EXAMPLES

Two examples are studied: the contact between a rigid plane with a cylinder and an ironing test. The first one aims at validating the behavior of the contact integration while the second one proposes to manage frictional condition in a more realistic example.

4.1 Contact between a cylinder and a plane

4.1.1 Hertz contact

Following the Hertz theory, one considers an elastic cylinder in contact with a plane under the small perturbation hypothesis. Frictionless contact is assumed. The governing equations of the Hertz theory are not reminded here (see [9] for details) but one get the following analytical solution for the contact pressure t_N:

$$t_N(x) = \frac{2P}{\pi a^2} \left(a^2 - x^2\right) = t_{N0} \left(1 - \frac{x^2}{a^2}\right)^{1/2} \tag{24}$$

$$\text{with:} \quad a = 2\sqrt{\frac{PR}{\pi E}} \tag{25}$$

where x, E, R, P and a denotes respectively the relative position of the contact point on the plane, the elastic modulus, the radius of the cylinder, the imposed pressure and the area of contact. The cylinder has a radius of $0.25\ m$ and steel material parameters are assumed. The external load on the cylinder is such that the maximum normal pressure is $1.e3\ Pa$.

Using symmetry, only a quarter of the cylinder is simulated. The computing mesh is represented in figure 2. It consists in 200*200 elements. The characteristic length of the elements is divided by 20 in each direction from the right top side to the left bottom side. The initial position of the cylinder is represented with a blue line. The boundary of symmetry is discretized with a conforming mesh for an easy application of the essential boundary conditions.

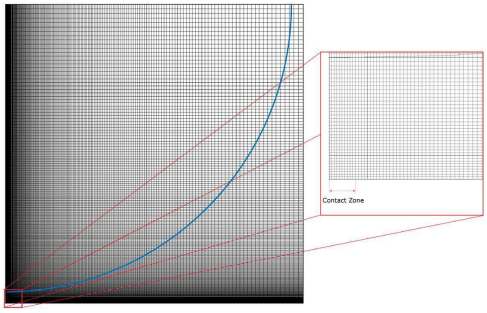

Figure 2: Mesh with a zoom on the cylindrical contact zone

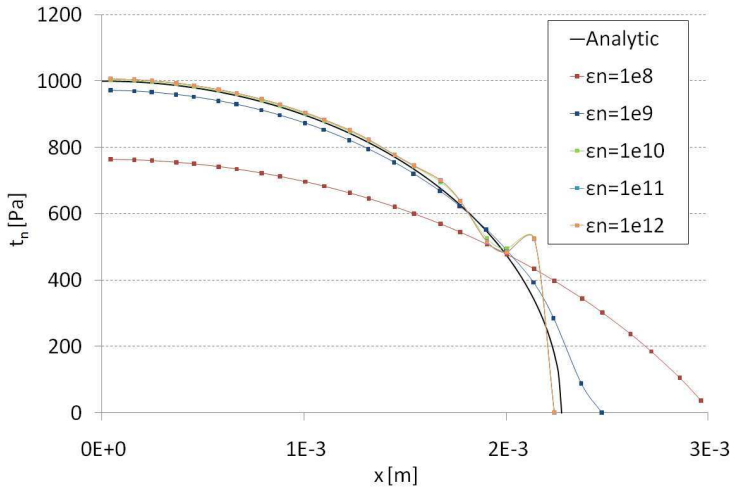

Figure 3: Contact normal stress as a function of the penalty parameter

Figure 3 presents the computed pressure on the plane as a function of the position. Various penalty parameters are tested. The contact integration using the penalty method follows the classical observations made in finite element simulations. If the penalty parameter is too small fast convergence is achieved and few mechanical iteration are needed but it leads to unphysical contact area and pressure. On the other hand, a too important penalty parameter improves the quality of the solution but reduce the convergence rate (for example, penalty parameter of 10^{12} requires three times as many iterations as a 10^{10} parameter for a similar solution).

4.1.2 Non-linear Hertz contact

The numerical strategy is now used on a large deformation elastoplastic cylinder with frictional contact on the interface. As the Hertz theory is invalid for such a situation, a classical finite element calculation is taken as a reference solution. The extended finite element mesh consists in a regular grid of 40*40 elements. The reference FEM calculation is performed using 1800 elements. Isotropic hardening is assumed. The yield stress and the hardening modulus are respectively set to $472\ MPa$ and $3000\ MPa$. The imposed displacement is equal to 12.5% of the radius. Figure 4 presents the corresponding Von-Mises stress in the structure.

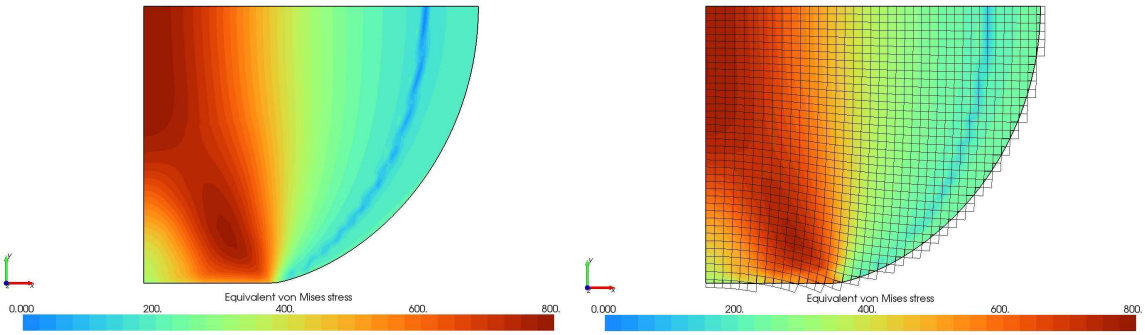

Figure 4: FEM solution (left) and X-FEM solution (right)

One can see that a good correlation between X-FEM and FEM simulations is achieved. The corresponding normalized forces on the tool are very close ($97.4\ N$ for the FEM model and $95.9\ N$ for the X-FEM).

4.2 Ironing test

As a more realistic metal forming example, one considers an ironing (or flattening) test depicted in figure 5. First, one imposes a vertical displacement of 12.5% of the initial height of the sheet to the tool. Next, an horizontal displacement of 66% of the length is imposed.

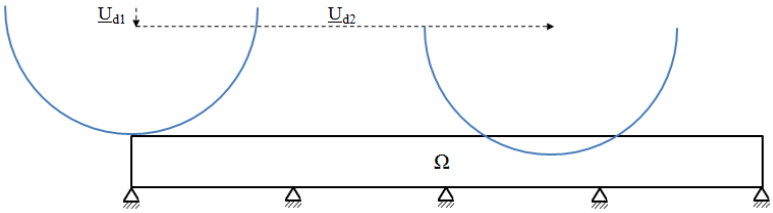

Figure 5: Ironing test

The material is the same than in the previous section. One assumes a frictional coefficient of 0.3. The length of the structure is $0.25\ m$ while the height is $0.02\ m$. The X-FEM mesh consists in 40*9 elements (only the upper line of elements is cut). The reference FEM mesh consists in 40*8 elements. To evaluate the accuracy of the contact integration, one compares the resulting forces on the tool in figure 6.

These graphics show the horizontal and vertical forces components on the tool (denoted respectively as FX and FY) for both the FEM and the X-FEM simulation. The right hand figure

represents the evolution of the forces during the vertical load U_{d1}. The left hand side represents the forces during the ironing phase U_{d2}.

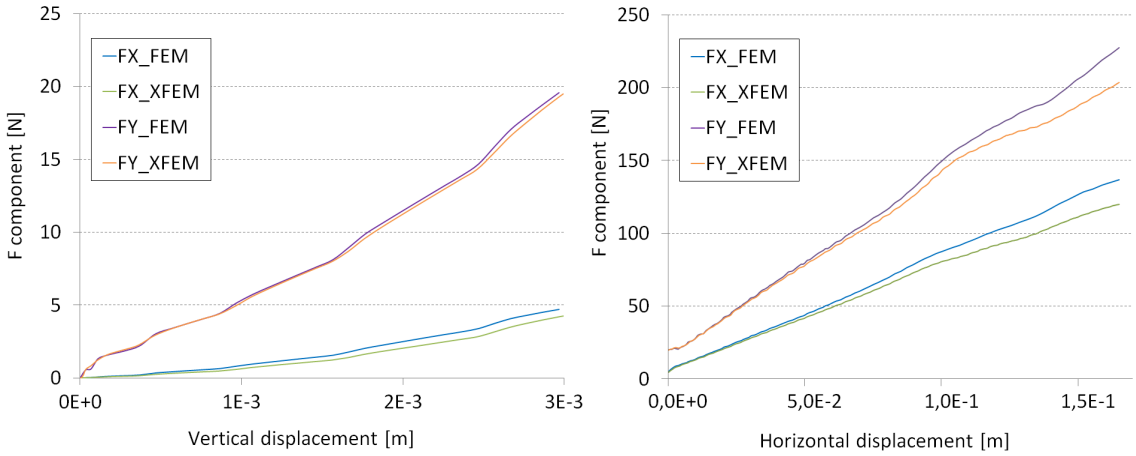

Figure 6: Evolution of the normal and tangential forces on the tool during; left hand: the normal load U_{d1}, right hand: the tangent load U_{d2}

The agreement between the X-FEM simulation and the FEM one is quite good (especially at the beginning of the simulation). One points out that for both simulations, if no specific strategy is used to manage the large deformations (e.g. the Arbitrary Lagrangian Eulerian formulation [10]), the mesh distortion becomes very important and even the FEM reference simulation validity may be questioned. One measures the mesh distortion using the maximum angle between the element edges (denoted as α) as:

$$\epsilon = \frac{\alpha - \pi/2}{\pi/2} \tag{26}$$

Then, a reference quadrangular element has a distortion of $\epsilon = 0$ while an element with two colinear edges have a distortion of $\epsilon = 1$. In the contact area, on gets a maximum element distortion of 0.991 for the X-FEM simulation and 0.982 for the FEM one. Whatever these distortions, the plastic strain field seems quite similar for both simulation.

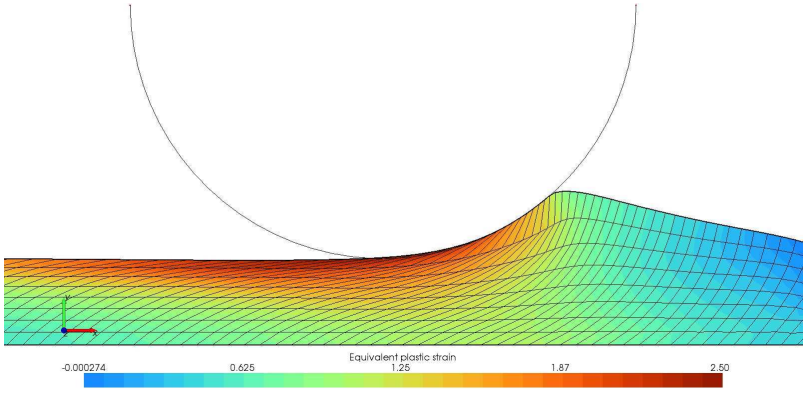

Figure 7: Ironing test - FEM solution

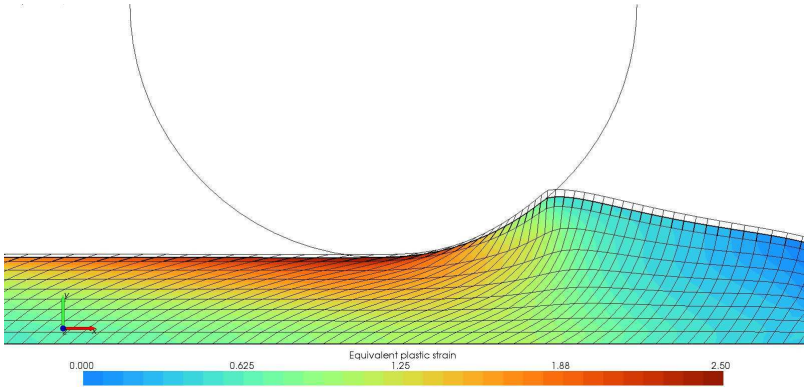

Figure 8: Ironing test - X-FEM solution

In figure 7 and 8, one represents the equivalent plastic strain in the contact zone for the FEM and the X-FEM simulations (respectively). In figure 8, the phantom nodes are plotted such that one can see the distortions of the extended finite elements. In future works, the Arbitrary Lagrangian Eulerian formulation should be implemented to improve the capabilities of the proposed strategy.

5 CONCLUSIONS

In the same way that the internal forces is sometimes computed using integration triangular sub-cells in the X-FEM [1], the contact loads on the structure may be computed using one-dimensional integration elements. Their Gauss points are employed within the two-dimensional quadrangular elements to compute the external contribution on each node and manage the behavior of the interface between the structure and the tool.

This strategy is very simple to handle as it is not subject to the same kind of instabilities than the ones that introduce dual unknowns in the formulation, as Lagrange multipliers method. Nevertheless, for contact problem formulations, attention should be paid to the penalty parameter values as in classical FEM calculations. Adaptive penalty strategies should help for industrial applications.

Numerical examples show the reliability of the approach to manage frictionless or Coulomb contact laws in the context of two-dimensional elasto-plastic large deformation analysis. However, independently of the contact formulation and for large deformations analysis, remeshing or Arbitrary Lagrangian Eulerian strategies should also be introduced to manage high distortions of the elements. It will be prospected in future works.

REFERENCES

[1] N. Moës, J. Dolbow, T. Belytschko: A finite element method for crack growth without remeshing. *International Journal for Numerical Methods in Engineering*, 46 (1999), 131–150.

[2] T.P. Fries, T. Belytschko: The extended/generalized finite element method: An overview of the method and its applications. *International Journal for Numerical Methods in Engineering*, 84 (2010), 253–304.

[3] N. Sukumar, D.L. Chopp, N. Moës, T. Belytschko: Modeling holes and inclusions by level sets in the extended finite element method. *Computer Methods in Applied Mechanics and Engineering*, 190 (2001), 6183–6200.

[4] S.E. Mousavi, N. Sukumar: Generalized Gaussian quadrature rules for discontinuities and crack singularities in the extended finite element method. *Computer Methods in Applied Mechanics and Engineering*, 199 (2010), 3237-3249.

[5] E. Béchet, N. Moës, B. Wohlmuth: A stable Lagrange multiplier space for stiff interface conditions within the extended finite element method. *International Journal for Numerical Methods in Engineering*, 78 (2009), 931–954.

[6] E. Pierres, M.C. Baietto, A. Gravouil: A two-scale extended finite element method for modelling 3D crack growth with interfacial contact. *Computer Methods in Applied Mechanics and Engineering*, 199 (2010), 1165-1177.

[7] J. Sethian: Level Set Methods and Fast Marching Methods: Evolving Interfaces in Computational Geometry, Fluid Mechanics, Computer Vision and Materials Science. Cambridge University Press, 1999.

[8] E. Biotteau, J.P. Ponthot: Modeling non-linearities in structural mechanics using the extended finite element method. *in preparation*.

[9] S. timoshenko, J.N. Goodier: Theory of elasticity (2nd edition). Mc Grawhill book company New-York, 1951.

[10] J. Donea, A. Huerta, J.P. Ponthot, A. Rodríguez-Ferran: Arbitrary Lagrangian-Eulerian Methods Encyclopedia of Computational Mechanics. John Wiley & Sons, Ltd, 2004.